International Journal of RF and Microwave Computer-Aided Engineering

WILEY

RESEARCH ARTICLE OPEN ACCESS

A Compact Low-Profile Multilayer Log-Periodic Metasurface Patch Antenna With Broadside Radiation

Mohamad Farran[1] | Mervat Madi[2] | Jihan Salah[3] | Antonio-D Capobianco[4] | Stefano Boscolo[5] | Karim Y Kabalan[6] | Obada Al-Khatib[2]

[1]Faculty of Sciences, Lebanese University, Nabatieh, Lebanon | [2]School of Engineering, University of Wollongong in Dubai, Dubai, UAE | [3]Communication Engineering Department, Sulaimani Polytechnic University, Sulaymaniyah, Iraq | [4]Department of Information Engineering, University of Padua, Padua, Italy | [5]DPIA Dipartimento Politecnico di Ingegneria e Architettura, Università degli Studi di Udine, Udine, Italy | [6]Electrical and Computer Engineering Department, The American University of Beirut, Beirut, Lebanon

Correspondence: Obada Al-Khatib (obadaalkhatib@uowdubai.ac.ae)

Received: 12 February 2026 | **Revised:** 31 May 2026 | **Accepted:** 13 June 2026

Academic Editor: Trushit Upadhyaya

Keywords: directive beams | log-periodic antenna arrays | metamaterial antennas | radiation patterns | wide-band antennas

ABSTRACT

A multilayer log-periodic metasurface patch antenna (LPMPA) operating in the 4–9-GHz frequency range with broadside radiation is presented. This antenna array is characterized by its compact size and low profile. Each element of the LPMPA consists of a 2-D periodic structure of 4×4 square patches, which can be viewed as a metasurface. The array is excited through aperture coupling in the ground plane beneath the radiators. The proper phase progression of the currents for a broadside radiation of the LPMPA's elements in the active region is obtained by increasing the length of the feed line placed between adjacent radiators. The structure's stop-band caused by the excess of length between radiators is eliminated by increasing the characteristic impedance of the feed line to 70 Ω in the proximity of each slot. A prototype of the proposed antenna, consisting of four 2-D periodic structures, is fabricated and tested. The obtained results show a 76% fractional bandwidth with gain ranges between 8 and 13 dB.

1 | Introduction

Log-periodic (LP) antennas are typically used for broadband applications where moderate gain is required [1]. Printed LP antennas can be designed for broadside radiation and nearly frequency-independent operation. The conventional method for designing a broadside printed LP antenna is to employ patch antennas as radiators [2–8]. Combining side-by-side patch antennas in an LP configuration results in wideband broadside radiation, but this comes at the expense of a large physical footprint. This is due to the large number of patches required to cover the desired frequency band, as patch antennas are inherently narrowband [2–8]. There are several papers in the literature discussing the size reduction of log-periodic dipole antennas (LPDAs); however, only a few have focused on the miniaturization of log-periodic patch antennas (LPPAs). Researchers have employed wideband antennas like bow-tie antennas [9] and fractal geometries [10, 11]. In [4], the authors used fractal-shaped patches for the LPPA size reduction, where 23% miniaturization was achieved. Several other types of LPPAs have also been proposed and are mainly distinguished by their feeding mechanism. The feeding mechanism can be either an inset feed [2, 3], a proximity feed [4–6], a gap coupling [7], or an aperture-coupled feed [8]. In these configurations, the scale factor is chosen large enough so that each array will have a large number of elements in order to overcome the disadvantage of the narrowband performance of microstrip patches.

Several techniques have been reported to overcome the narrow bandwidth of a single-patch antenna [12–15]. Most of these techniques cannot be easily applied in the design of an LP array. A broadband and low-profile patch antenna design based on composite right-/left-handed (CRLH) capacitors or mushroom periodic structures has been proposed in [16, 17]. These periodic structures are easily implemented in an LP configuration, which consists of several two-dimensional metamaterial structures and can be viewed as an LP metasurface (MS). Recent research has highlighted the emergence of MS-based LP antennas as an innovative and effective category. These designs leverage frequency-scaled unit cells, modulated impedance, and multilayer MS architectures to achieve both compactness and broad operational bandwidth [18–22]. For instance, Amini et al. [20] introduced a modulated MS leaky-wave antenna that was optimized through interpretable AI methodologies, whereas Pang et al. [21] showcased a grounded dielectric MS antenna that features an expansive field of view and significant gain. These studies provide evidence that MS-based LP configurations can successfully address the challenges associated with narrowband patch antennas.

The antenna proposed in this paper builds on these advancements by integrating four 2-D MS structures with a scale factor of 0.88, presenting a compact and highly efficient solution. The design presented herein consists of a sequence of side-by-side 2-D periodic structures based on a series of capacitor unit cells. In an LP patch configuration, it is not possible to add 180° phase to the terminal of each patch by crisscrossing the feed line as in an LP dipole array. The effect of crisscrossed feed can be accounted for by using longer feed lines, which results in a structural stop-band [23, 24]. This nonpropagation region is eliminated by modulating the characteristic impedance of the feed line in the proximity of each radiator [23]. The LP design, presented in this paper, is made of four 2-D structures or four MS, and is fed through aperture coupling using a modulated microstrip line and four slots etched in the ground plane. The antenna is designed to work in the 4–9-GHz frequency range. A scale factor τ of 0.88 is used, resulting in a compact design. The overall dimension of the proposed antenna is $40 \times 110\,\text{mm}^2$. The results demonstrate a stable broadside radiation pattern, with a gain range of 8–13 dB and an efficiency of 87%. The examples presented in [2–8], where the scale factor is large, use more radiators, a more complex design, less compact, and a lower efficiency. To highlight the novelty of the proposed antenna, we will compare it with the recent works in the literature where the size reduction of an LPPA is discussed. In [4], an LPPA is proposed with a bandwidth of 7.5 GHz; the feed is a proximity type, and fractal patch squares are used to reduce the antenna dimensions. Fifteen patches are employed with a scale factor $\tau = 0.92$, resulting in overall dimensions of $173 \times 70\,\text{mm}^2$. The large number of patches required to cover the desired frequency band leads to beam squint in the radiation pattern. The reported gain ranges between 8 and 10 dB, with a radiation efficiency of about 80%. In comparison, our proposed antenna achieves a higher midband gain, peaking at 13 dB.

In [5], an artificial magnetic conductor (AMC) is used as a ground plane to reduce the size of the LPPA. Eleven patches are employed with $\tau = 0.93$, covering the band from 5.3 to 8 GHz. The patches are fed by a proximity type, and the overall size of the antenna is $50 \times 122.5\,\text{mm}^2$. However, the AMC concept results in a very complex structure. The antenna presented in [8] is similar to our design, where an aperture-coupled feed is used. The structure contains 20 square patches that cover the band from 7 to 10 GHz, with overall dimensions of $50 \times 280\,\text{mm}^2$. The measured gain ranges from 9.83 to 14.54 dB, with a peak of 16.42 dB at midband, showing a trend consistent with the gain behavior observed in our work.

The multilayer LPMPA (log-periodic metasurface patch antenna) introduced in this paper offers superior impedance matching and extended frequency coverage without compromising size or efficiency. Compared with the antenna presented in [8], the proposed LPMPA is considerably more compact, even though it operates over a higher frequency band (4–9 GHz). Its performance surpasses earlier designs in terms of bandwidth, compactness, radiation pattern stability, and efficiency.

The remainder of this paper is organized as follows: Section 2 details the design methodology of the multilayer LPMPA. Section 3 describes the feed network design. Section 4 presents the measurement results and discusses both theoretical and experimental findings. Finally, Section 5 concludes the paper.

2 | Multilayer LPMPA Design

The structure of the multilayer LPMPA antenna is illustrated in Figure 1. The detailed dimensions will be defined later. This antenna is based on three metal layers separated by two dielectric substrates, which are both Rogers RO4003C with a relative permittivity of 3.45 and a loss tangent of 0.0027. The top metal layer consists of four 2-D structures, each formed of $m \times m$ unit cells, where $m = 4$ is the number of capacitors along the x-axis and y-axis directions. The 2-D periodic structures are printed on the top substrate, which has a thickness of 3.04 mm.

Four slots are etched in the full ground plane of this first substrate. A modulated microstrip feed line with 50-Ω input impedance is printed at the bottom of the second 0.812-mm-thick substrate. Each $m \times m$ capacitors group is excited through a slot etched in the ground plane right beneath. The dominant mode TM_{10} and the second-order mode TM_{20} are simultaneously excited in each 2-D periodic structure, leading to broadband directive radiation [23]. Numerical simulations demonstrate that the fractional bandwidth of each 2-D periodic structure antenna is almost 28%, as in [23]. This large bandwidth allows the use of a small scale factor and have a few radiating elements, unlike several works in the literature where a huge number of elements are used. In this work, the resonance frequencies of adjacent TM_{10} and TM_{20} modes of all 2-D structures and other parameters are related by the scale factor ∬, where

$$\frac{1}{\tau} = \frac{w_n}{w_{n+1}} = \frac{s_n}{s_{n+1}} = \frac{l_n}{l_{n+1}} = \frac{p_n}{p_{n+1}} = \frac{d_n}{d_{n+1}} = \frac{d'_n}{d'_{n+1}} \quad (1)$$

w_n and s_n are the lateral dimensions of the nth 2-D structure (TM_{10} mode) and the mth capacitor (TM_{20} mode), respectively. l_n is the slot length located right beneath the nth 2-D structure, w_s is the slot width and is not subject to the scale factor. p_n is the period of the unit cell in the nth 2-D structure and is equal to $s_n + g$, where g is the gap width between unit cells; g is not subjected to the scale factor. d_n is the length of nth cell, which contains the $m \times m$ patches, and d is the length of the subcell feed line, which will be discussed in the next section. The proposed LP antenna

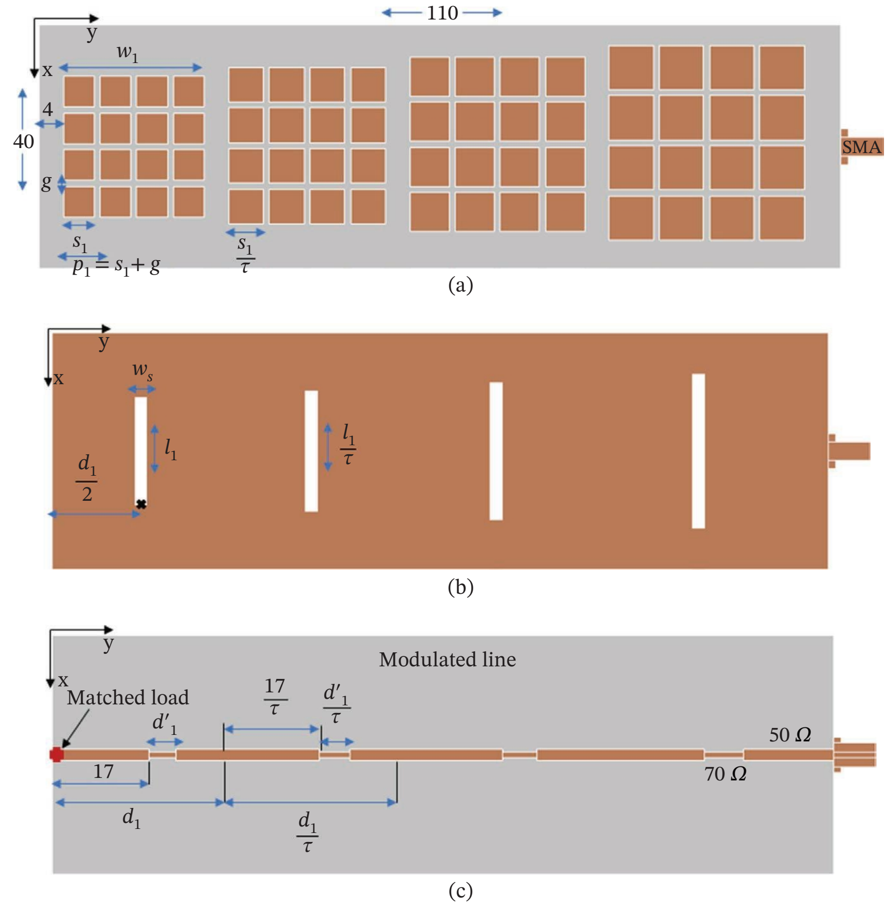

FIGURE 1 | Multilayer log-periodic metasurface patch antenna (LPMPA) (dimensions in mm, and $\tau = 0.88$): (a) top view: log-periodic 2-D periodic structures; (b) middle metal layer: aperture coupling feeding structure; (c) bottom view: modulated microstrip.

TABLE 1 | Dimensions of 2-D structures (MS) and their distances from the feed point.

MS number (n)	Dimension of MS $w_n \times w_n$ (mm^2)	Dimension of unit cell $s_n \times s_n$ (mm^2)	Slot length: l_n (mm)	Distance from the center of MS (or slot) to the feed point(mm)
$n = 4$	31.85×31.85	7.21×7.21	25.92	21.93
$n = 3$	28.53×28.53	6.38×6.38	22.98	56.13
$n = 2$	25.6×25.6	5.65×5.65	20.34	87.2
$n = 1$	23×23	5×5	18	116

structure is intended to work in the 4–9-GHz frequency range. The dimensions of the smallest 2-D periodic structure ($n = 1$) are determined for the higher frequency limit of the band (9 GHz) as follows: $s_1 = 5$ mm, $w_1 = 23$ mm, and $g = 1$ mm (see Figure 1a). The dimensions of the first slot are: length $l_1 = 18$ mm, and width $w_s = 2$ mm (see Figure 1b). The length of 1st cell is $d_1 = 30$ mm, and of the 1st subcell $d = 3.5$ mm. More details of the design are shown in Table 1.

In [16] and [17], authors demonstrate that the transmission-line model applies to the mode analysis, and here is another advantage of using these CRLH capacitor structures in an LP configuration. Practically, it is possible to predict the resonance frequencies for the TM_{10} and TM_{20} modes of all the 2-D structures in the array, and this happens once the scale factor is applied to the first chosen element. In our case the highest frequency element is chosen as the 1th. We can use the equations below as in [16] and [17] to predict the resonance frequencies of the dominant mode TM_{10}, and the second order mode TM_{20} of each 2-D periodic structure that form the multilayer LPMPA:

$$\frac{\beta_{cu} p}{\pi} = \frac{1 - 2\beta_{\text{eff}} \Delta L/\pi}{m}, TM_{10} \text{ mode} \quad (2)$$

$$\frac{\beta_{cu} p}{\pi} = \frac{1 - 2\beta_{\text{eff}} \Delta L/\pi}{m/2}, TM_{20} \text{ mode} \quad (3)$$

$$\beta_{\text{eff}} = k_0 \frac{\sqrt{\varepsilon_{\text{eff}}}}{c} = 2\pi f \frac{\sqrt{\varepsilon_{\text{eff}}}}{c} \tag{4}$$

$$\frac{\Delta L}{h} = 0.412 \frac{(\varepsilon_{\text{eff}} + 0.3)(w/h + 0.262)}{(\varepsilon_{\text{eff}} - 0.258)(w/h + 0.813)} \tag{5}$$

$$\varepsilon_{\text{eff}} = \frac{\varepsilon_r + 1}{2} + \frac{\varepsilon_r - 1}{2}\left(1 + \frac{12h}{w}\right)^{-1/2} \tag{6}$$

where p, w, and m represent the same parameters defined before for the multilayer LPMPA: period of the unit cell, width of the 2-D structure, and the number of capacitors in each 2-D structure. In our case, $m = 4$. h is the height of the first substrate and is equal to 3.04 mm. k_0, f, and c represent the wavenumber in free space, the operating frequency, and the speed of light in vacuum, respectively.

The propagation constants are defined as follows:

- β_{cu} denotes the propagation constant of the capacitor unit cell, which can be extracted from the S-parameters and the ABCD matrix.
- β_{eff} represents the effective propagation constant when the patch dimensions are extended due to the fringing field effect.

This extension introduces an additional length ΔL at each end along the resonant direction, which in this case corresponds to the y-direction.

By using the simulation model included in Figure 2, we can calculate numerically the dispersion curve of the capacitor unit cells. The resonant frequencies of the dual modes of all antennas in the LP structure can be estimated by plotting the right-hand side expressions of 2 and 3 as in Figure 2, where we have analyzed the dispersion curves of the higher and lower frequency antennas ($n = 1, 4$) in the LP structure. We can note that in Figure 2 the dominant TM_{10} and the second-order mode TM_{20} are located on the right-handed dispersion branch of the CRLH in case ($n = 1, 4$). Consequently, the two 2-D structures ($n = 2, 3$) in the middle have the same properties. Thus, the resonant peaks will sum up, leading to broadband operation of this type of periodic structure. The scaling factor ($\tau = 0.88$) is applied to all the remaining 2-D structures. Table 2 shows the predicted resonant frequencies for all antennas in the LPMPA structure, where very close resonant peaks appear between different modes of the four 2-D structures.

3 | Feed Network Design

Figure 2 shows the dispersion curve or the relationship between $(\beta_{cu}\rho)/\pi$ and the frequency, where it can be readily seen that the stop-band is located between the lower and the upper bands, delimited by the two frequencies f_{c1} and f_{c2}. It can also be noticed from Figure 2a,b that f_{c1} is almost equal (= 4.45 GHz) in the two cases of the elements of higher and lower frequencies. The frequency f_{c2} is larger for the higher frequency element, and this causes a larger stop-band. In the

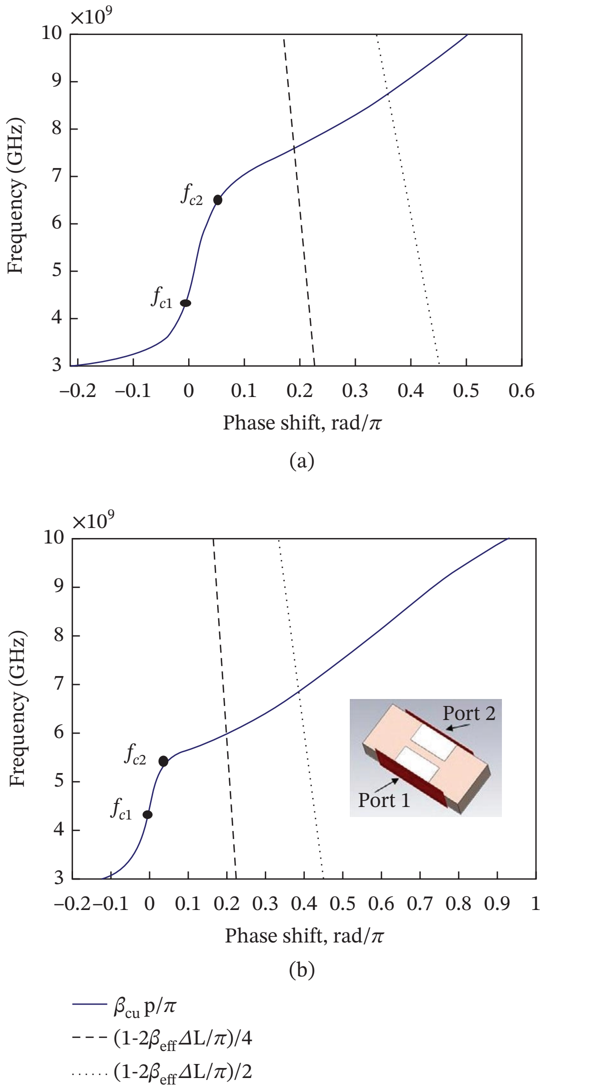

FIGURE 2 | Dispersion diagram of the capacitors unit cell. (a) High-frequency element and (b) low-frequency element.

TABLE 2 | Predicted resonance frequencies for all antennas in the LPMPA structure.

2-D structure	(1)	(2) $(1/\tau)$	(3) $(1/\tau^2)$	(4) $(1/\tau^3)$
TM_{10} (GHz)	7.58	7.03	6.51	5.98
TM_{20} (GHz)	8.73	8.07	7.45	6.83

stop-band, no wave can propagate along the structure. The energy flows at the input point, causing an appreciable impedance mismatch. As a result, the LPMPA should be excited at the low-frequency end. Simulations demonstrate that by exciting the antenna at the high-frequency end, the lower cut-off frequency of the LPMPA is 6.5 GHz. Instead, if it is excited at the lower frequency end, the cutoff frequency is 4.25 GHz. Now, let us consider the radiating LP structure in Figure 1 as a cascade of $n = 4$ single cells that are related one to the other in a LP manner. Each unit cell of the LPMPA structure consists of a length d_n of the feed line, $m \times m$ patches fed by the energy coupling through the slot with length l_n beneath the patches of the cell (see Figure 1c). A numerical optimization procedure involving the fine-tuning of the characteristic impedance and the length of the modulated section leads to the value and the length of the subcell transmission line d'_n (see Figure 1c where $d'_1 = 3.5\,\text{mm}$). The impedance of the 50-Ω microstrip feeding line is increased to 70 Ω in the proximity of each slot to approximately match each $m \times m$ section of patches to 50 Ω. Furthermore, we noticed that the relative impedance between cells and the feeding line is easily adjusted by offsetting the position of the modulated part of the feed line from the center line of the slot (see Figure 1b,c).

4 | Measurement Results and Discussion

Figure 3a,b show the multilayer LPMPA prototype after its fabrication. The total antenna size is $40 \times 110 \times 3.852\,\text{mm}^2$. The 50-Ω matched load is not necessary because most of the power we pump in is radiated; it only helps to perfect the reflection coefficient at some frequencies. The simulated (dashed line) and measured (solid line) magnitudes of S11 for multilayer LPMPA with and without the 50 Ω matched load are compared in Figure 4. This reveals a good agreement and impedance matching with a −10-dB fractional bandwidth of 76%. The antenna operates over a frequency range from 4 to 9 GHz with realized gain ranging from 8 to 13 dB (see Figure 4), and the numerically computed efficiency is around 87% in all the operating bands. The measured E-plane and H-plane patterns at several frequencies within the operating band are plotted in Figure 5. It is observed that the maximum beam is slightly tilted away from the broadside direction (z-axis) at certain frequencies (see Figure 5a,c). The peak gain direction is confined within 10° from the z-axis due to the pattern tilting, which is $< 5°$ within the 5.5–7.5-GHz frequency range. The measured peak gains of the multilayer LPMPA are much higher than would be expected from an LP dipole or patch of the same parameters; it is $> 10\,\text{dB}$ in the ranges of 5–8 GHz and around 8 dB outside this range (see Figure 4). The far-field is almost linearly polarized, since the measured cross-polarization components are always 25 dB smaller than the copolarization components. A discrepancy is observed between the simulated and measured results, which can be attributed to several practical factors. First, fabrication tolerances introduced during manual assembly in the university laboratory, particularly in the alignment and bonding of multilayer structures using adhesive materials, may lead to deviations from the ideal design.

To enhance the understanding of the proposed antenna performance, a comparative analysis is provided in Table 3, focusing on the evolution from conventional LP designs [1] to the proposed multilayer LPMPA. The proposed antenna integrates MS wave manipulation with LP scaling to achieve a superior trade-off between fractional bandwidth (76%), stable broadside

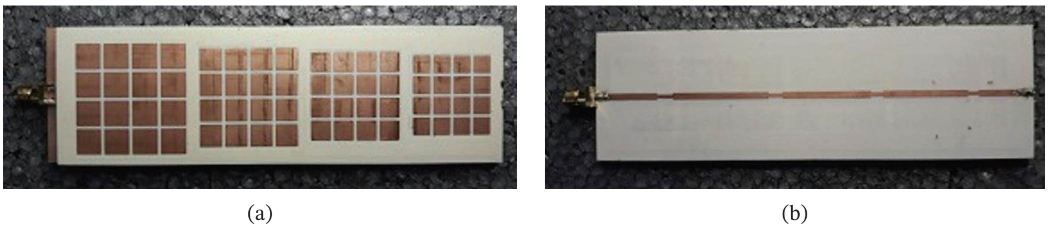

FIGURE 3 | Prototype of the proposed antenna: (a) top view and (b) bottom view.

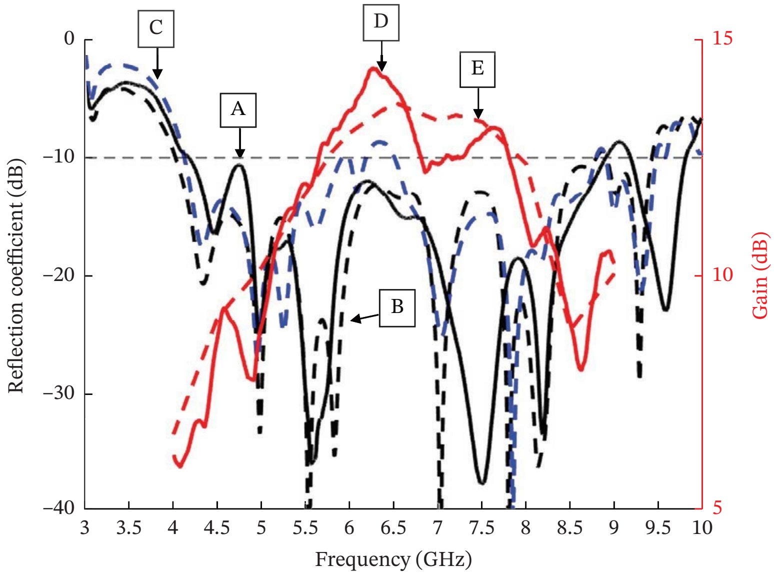

FIGURE 4 | Reflection coefficient: (A) measured (black solid lines), (B) computed with 50-Ω matched load (black dashed lines), and (C) computed without matched load at the end of the feed line (blue dashed lines). Gain: (D) the measured gain (solid red lines) and (E) the computed gain (dashed red lines).

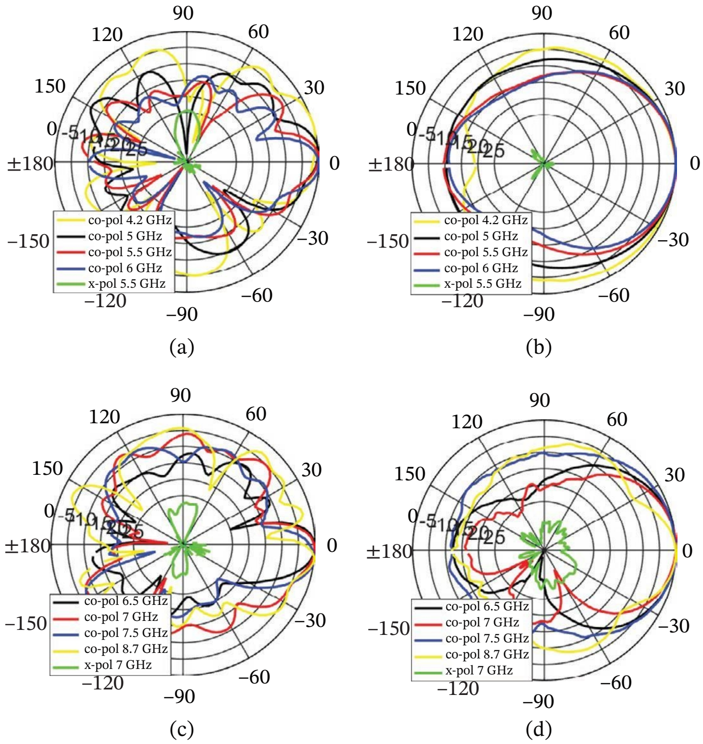

FIGURE 5 | Measured radiation patterns of the broadside multilayer LPMPA array. The green line shows the measured cross-polarization component. The display scale is from −40 to 0 dB (5 dB per division). (a, c) E-plane: Angles are measured starting from the *z*-axis towards the *y*-axis; (b, d) H-plane: Angles are measured starting from the *z*-axis towards the *x*-axis.

TABLE 3 | Comparative analysis of the proposed LPMPA with log-periodic designs.

Ref.	Frequency	FBW (%)	Gain (dB)	Antenna type	Size (λ_0)
[4]	(3.1–10.6)	110%	8–10	LPPA (one layer)	$\sim 3.95 \times 1.6$
[5]	(5.3–8)	40.6%	4.53–7.57	LPMA + AMC packing	$\sim 2.71 \times 1.11$
[8]	(7–10)	35.3%	9.83–14.54 (16.4 pk)	Reconfigurable LPPA (aperture-coupled, planar array)	$\sim 7.93 \times 1.42$
[20]	18	~60	6–10	Single-layer metasurface antenna	$\sim 0.65 \times 0.65$
[21]	10	N/A	16.5	Multilayer metasurface antenna (lens-based)	$\sim 0.1 \times 7$
[22]	(4.1-5.4)	~50	7–11	Dual-layer metasurface antenna	$\sim 0.6 \times 0.6$
[25]	(12, 13, 15, 16, 18, 23, 24)	60.0	6–10	Single-layer metasurface antenna	$\sim 0.65 \times 0.65$
[26]	(4.7–6.4)	45.0	Up to 9.9	Multilayer metasurface antenna (review)	Flexible ($\geq 0.7 \times 0.7$)
This Work	(4–9)	76.0	8–13	Multilayer log-periodic metasurface patch antenna (LPMPA)	2.38×0.87

gain (8–13 dB), and a compact electrical size of $2.38 \times 0.87\ \lambda_0$ Compared directly with standard LPPAs [2–8], which typically exhibit significantly larger radiating apertures or lower gain profiles within similar microwave frequency ranges, the proposed LPMPA maintains high performance while achieving substantial miniaturization.

Although various existing MS designs provide unique wave manipulation capabilities—such as AI-optimized modulated structures at 18.0 GHz [20], lens-based dish equivalents at 10.0 GHz [21], circularly polarized designs across 4.1–5.4 GHz [22], Ku-band aerospace phased arrays at 12.0–18.0 GHz [25], and dual-layer miniaturized configurations (DUMA) operating across 4.7–6.4 GHz [26]—they generally lack the combined extreme wideband performance (76.0%) and LP scaling advantages demonstrated in this work.

Our proposed antenna, however, achieves a much larger FBW of 76% and a gain between 8 and 13 dB, all within a compact multilayer design measuring only $2.38 \times 0.87\ \lambda_0$. The multilayer MS configuration offers multiple advantages: broader bandwidth, improved impedance matching, and higher radiation efficiency, while supporting complex geometries like LP MSs without increasing overall size. Nevertheless, multilayer designs pose challenges such as fabrication complexity, higher costs, and alignment difficulties during assembly. Despite these challenges, the significant benefits in bandwidth and gain make our multilayer design an excellent choice for advanced microwave applications needing compact, wideband, and high-efficiency antennas. This comparison highlights the innovation and importance of our design relative to existing state-of-the-art solutions.

5 | Conclusions

A compact LPPA was developed based on the concept of a CRLH capacitor unit cells. The capacitors' unit cells are easily implemented in an LP configuration, which consists of several two-dimensional metamaterial structures and can be viewed as an LP MS. The transmission-line model integrated with the dispersion relation of the capacitor unit cells has been applied to perform the feed line and to predict the dual operating modes for each 2-D structure. The proposed antenna exhibits a 76% fractional bandwidth. The reflection coefficient and far-field patterns were numerically calculated and experimentally measured, showing good agreement. The multilayer LPMPA exhibits a higher gain than would be obtained from an LPDA or LPPA of the same parameters. This compact broadband radiator can be employed in radar and wireless communication systems.

Acknowledgments

This project has been jointly supported with the support of the National Council for Scientific Research in Lebanon CNRS-L, Lebanese University, and American University of Beirut.

Funding

This study was supported by the American University of Beirut Research Board (Grant Number 104552). Open access publishing was facilitated by University of Wollongong, as part of the Wiley-University of Wollongong agreement via the Council of Australasian University Librarians.

Conflicts of Interest

The authors declare no conflicts of interest.

Data Availability Statement

Data sharing is not applicable to this article as no datasets were generated or analyzed during the current study.

References

1. C. A. Balanis, *Antenna Theory: Analysis and Design*, 3rd ed. (Wiley, 2005).

2. M. Dadel, and S. Srivastava, *Arrays of Patch Antenna Using Log Periodic Property* (Indian Antenna Week (IAW), 2011), https://doi.org/10.1109/IndianAW.2011.6264943.

3. S. A. Nasir, S. Arif, M. Mustaqim, and B. A. Khawaja, "A Log-Periodic Microstrip Patch Antenna Design for Dual Band Operation in Next Gener-Ation Wireless Lan Applications," in *IEEE 9th International Conference on Emerging Technologies (ICET)* (IEEE, 2013), 1–5, https://doi.org/10.1109/ICET.2013.6743498.

4. A. Amini, and H. Oraizi, "Miniaturized UWB Log-Periodic Square Fractal Antenna," *IEEE Antennas and Wireless Propagation Letters* 14 (2015): 1322–1325, https://doi.org/10.1109/LAWP.2015.2411712.

5. A. T. Almutawa, and G. Mumcu, "Small Artificial Magnetic Conductor Backed Log-Periodic Microstrip Patch Antenna," *IET Microwaves, Antennas & Propagation* 7, no. 14 (2013): 1137–1144, https://doi.org/10.1049/iet-map.2013.0028.

6. S. H. Anuar, M. T. Ali, N. H. K. Anuar, A. L. Yusof, and M. N. Md Tan, "Design and Analysis of a Log Periodic Antenna by Using Proximity Fed Network," in *IEEE Control and System Graduate Research Colloquium* (IEEE, 2012), 70–75.

7. M. Dadel, K. P. Tiwary, and S. Srivastava, "Log Periodic Triangular Patch Antenna With Gap Coupled Feed," in *International Conference on Signal Processing and Communication (ICSC)* (IEEE, 2015), 99–104.

8. M. R. Hamid, P. S. Hall, and P. Gardner, "Frequency Reconfigurable Log Periodic Patch Array," *Electronics Letters* 46, no. 25 (2010): 1648–1650, https://doi.org/10.1049/el.2010.2941.

9. L. Shu, L. Hongmei, Q. Jinghui, and Y. Qidi, "A Log-Periodic Bow-Tie Dipole Antenna," in *5th International Conference on Microwave Electronics: Measurement, Identification, Applications* (Harbin Institute of Technology, 2005), 58–61.

10. N. S. M. Yaziz, M. K. A. Rahim, and F. Zubir, "Second Iteration of Slotted Fractal Log Periodic Dipole Antenna (LPDA)," in *International Symposium on Antennas and Propagation (ISAP)* (IEEE, 2017).

11. M. C. Özgönül, and M. Seçmen, "Size-Reduced Printed Log Periodic Dipole Antenna With Single First Order Semi-Circle Iteration and Feed Point Patches," in *International Symposium on Antennas and Propagation (ISAP)* (IEEE, 2017).

12. K. M. Luk, C. L. Mak, Y. L. Chow, and K. F. Lee, "Broadband Microstrip Patch Antenna," *Electronics Letters* 34, no. 15 (1998): 1442–1443, https://doi.org/10.1049/el:19981009.

13. S. D. Targonski, and D. M. Pozar, "Design of Wideband Circularly Polarized Aperture-Coupled Microstrip Antennas," *IEEE Transactions on Antennas and Propagation* 41, no. 2 (1993): 214–220, https://doi.org/10.1109/8.214613.

14. F. Croq, and A. Papiernik, "Stacked Slot-Coupled Printed Antenna," *IEEE Microwave and Guided Wave Letters* 1, no. 10 (1991): 288–290, https://doi.org/10.1109/75.89098.

15. D. Sun, W. Dou, L. You, X. Yan, and R. Shen, "A Broadband Proximity-Coupled Stacked Microstrip Antenna With Cavity-Backed Configuration," *IEEE Antennas and Wireless Propagation Letters* 10 (2011): 1055–1058, https://doi.org/10.1109/LAWP.2011.2169389.

16. W. Liu, Z. N. Chen, and X. Qing, "Metamaterial-Based Low-Profile Broadband Aperture-Coupled Grid-Slotted Patch Antenna," *IEEE*

Transactions on Antennas and Propagation 63, no. 7 (2015): 3325–3329, https://doi.org/10.1109/TAP.2015.2429741.

17. W. Liu, Z. N. Chen, and X. Qing, "Metamaterial-Based Low-Profile Broadband Mushroom Antenna," *IEEE Transactions on Antennas and Propagation* 62, no. 3 (2014): 1165–1172, https://doi.org/10.1109/TAP.2013.2293788.

18. W. E. I. Liu, Z. N. Chen, X. Qing, J. Shi, and F. H. Lin, "Miniaturized Wideband Metasurface Antennas," *IEEE Transactions on Antennas and Propagation* 65, no. 12 (2017): 7345–7349, https://doi.org/10.1109/TAP.2017.2761550.

19. T. Huang, S. Huang, Z. Wen, et al., "Multifunctional Metasurface Based on Cascaded Multilayer Modules," *Nanomaterials* 15, no. 20 (2025): 1563, https://doi.org/10.3390/nano15201563.

20. A. Amini, A. Moshiri, M. A. C. Zadeh, and V. Nayyeri, "Interpretable Artificial Intelligence for Modulated Metasurface Antenna Design Using Shap and MLP," *Scientific Reports* 15, no. 1 (2025): 24029, https://doi.org/10.1038/s41598-025-10156-1.

21. K. Pang, Y.-J. Xie, W.-K. Si, P.-Y. Wu, and S. Chen, "On-Demand High Gain And Directional Surface Wave Antenna With 100° Field of View Based On Grounded Dielectric Metasurface," *Applied Physics Letters* 126, no. 25 (2025): 251703, https://doi.org/10.1063/5.0272683.

22. Y. Wang, Z. Ding, J. Yu, et al., "Metasurface-Based Circularly Polarised Antenna: Enhanced Bandwidth With Characteristic Mode Analysis and Symmetric Branch Design," *IET Microwaves, Antennas Propagation* 18, no. 12 (2024): 974–984, https://doi.org/10.1049/mia2.12516.

23. P. Ingerson, and P. Mayes, "Log-Periodic Antennas With Modulated Impedance Feeders," *IEEE Transactions on Antennas and Propagation* 16, no. 6 (1968): 633–642, https://doi.org/10.1109/TAP.1968.1139275.

24. M. David, *Pozar, Microwave Engineering*, 4th ed. (John Wiley & Sons, 2012).

25. D. Astaire, and P. Hay, "Impacts of Metasurface Antenna Technology in the Aerospace Industry," in *AIAA Region II Conference* (Aerospace Research Central, 2025)99728.

26. A. K. Iyer, A. Alù, and A. Epstein, "Metamaterials and Metasurfaces - Historical Context, Recent Advances, and Future Directions," *IEEE Transactions on Antennas and Propagation* 68, no. 3 (2020): 1223–1231, https://doi.org/10.1109/TAP.2020.2969732.